



Geological Characteristics and Exploration Prospect of Black Shale in the Dongyuemiao Member of Lower Jurassic, the Eastern Sichuan Basin, China

Guodong Wei^{1,2,3}, Wei Wang^{1,2*}, Liang Feng⁴, Xiucheng Tan^{3*}, Chuan Yu^{1,2}, Hualian Zhang^{1,2}, Zhiping Zhang^{1,2} and Shengxiu Wang^{1,2}

OPEN ACCESS

Edited by:

Feng Yang,
China University of Geosciences
Wuhan, China

Reviewed by:

Qilu Xu,
China University of Petroleum, China
Zhipeng Huo,
Northeastern University at
Qinhuangdao, China
Xianfeng Tan,
Chongqing University of Science and
Technology, China

*Correspondence:

Wei Wang
cqdyysg_ww@126.com
Xiucheng Tan
tanxiucheng70@163.com

Specialty section:

This article was submitted to
Economic Geology,
a section of the journal
Frontiers in Earth Science

Received: 27 August 2021

Accepted: 15 October 2021

Published: 10 November 2021

Citation:

Wei G, Wang W, Feng L, Tan X, Yu C,
Zhang H, Zhang Z and Wang S (2021)
Geological Characteristics and
Exploration Prospect of Black Shale in
the Dongyuemiao Member of Lower
Jurassic, the Eastern Sichuan
Basin, China.
Front. Earth Sci. 9:765568.
doi: 10.3389/feart.2021.765568

¹Key Laboratory of Shale Gas Exploration, Ministry of Natural Resources, Chongqing Institute of Geology and Mineral Resources, Chongqing, China, ²National and Local Joint Engineering Research Center of Shale Gas Exploration and Development, Chongqing Institute of Geology and Mineral Resources, Chongqing, China, ³School of Geoscience and Technology, Southwest Petroleum University, Chengdu, China, ⁴Chongqing Gas Field, PetroChina Southwest Oil and Gas Field Company, Chongqing, China

China has yielded huge commercial production from the marine organic-rich shale but shows a slow exploration process in the lacustrine organic-rich shale. Multiple lacustrine shales in the Lower Jurassic of the eastern Sichuan Basin, rich in organic matters, are potential targets for shale hydrocarbon exploration and development. An investigation of the Dongyuemiao member, Lower Jurassic, was firstly conducted utilizing the macroscopic and microscopic analyses on outcrops and drilling cores to reveal the characteristics of sedimentary subfacies, mineral compositions, organic matter content and types, thermal maturity level, and reservoir quality. The dark shales in the Dongyuemiao member can be grouped into four general categories: shore, shallow, semi-deep, and deep lacustrine shales. The semi-deep and deep lacustrine shales generally have higher values in thickness (>20 m), average total organic carbon (TOC) content (>1.5 wt.%), and average porosity (>2%) relative to shore and shallow lacustrine shales. All four categories of shales primarily consist of type II kerogen and have thermal maturity levels exceeding the vitrinite reflectance value of 0.9–1.0% (or the T_{max} of ~440°C). Thermally powered pore generation generally promoted the pore system as indicated by the positive correlation between porosity and T_{max} . Notably, the semi-deep lacustrine shale in the vicinity of the Qiyueshan Fault Zone shows abnormally high porosity and low oil saturation index (OSI) at T_{max} > ~465°C potentially due to the promoted hydrocarbon expulsion through multiscale fractures. Except for the vicinity of the Qiyueshan Fault Zone, the semi-deep and deep lacustrine shales generally show the better exploration prospect relative to the shore and shallow lacustrine shales. Additionally, the high content of clay minerals (>40 wt%) reduced the brittleness of the semi-deep and deep lacustrine shales which may challenge the artificial hydraulic fracturing.

Keywords: shale porosity, oil saturation index, lacustrine shale, Dongyuemiao member, sichuan basin

INTRODUCTION

According to the suggestion of IPCC, global warming should be essentially limited to a threshold of 1.5°C by the mid-21st century to prevent dangerous climate change. To achieve the peak CO₂ emissions before 2030 and the carbon neutrality before 2060, China has stepped up the exploration and development of clean energy, and natural gas is an important part of energy conversion.

Unconventional shale gas is the main growth point of China's natural gas resource in the last decade. For instance, the Wufeng-Longmaxi Shale in South China has yielded a proven geological reserve of >2 trillion cubic meters and an annual output of >20 billion cubic meters in 2020, making China the largest shale gas production region outside North America (He and Zhu, 2012; Li et al., 2015; Wang et al., 2015; Liu et al., 2017; Dong et al., 2018; Chen et al., 2020; Qiu et al., 2020). More recently, the exploration and development of lacustrine shale gas in the Fuling and Yuanba areas of the Sichuan Basin (southwestern China) and the Yanchang Formation of the Ordos Basin (northern China) have well developed. Thereinto, the shale gas resources of the organic-rich shale in the Ziliujing Formation (Lower Jurassic) of the Sichuan Basin were estimated to be > 1 trillion cubic meters (Zhang et al., 2008; Zou et al., 2019a), indicating a very substantial exploration prospect.

Nevertheless, the organic-rich shale in the Ziliujing Formation was deposited in the lacustrine environment. Compared with the stable sedimentary environment of marine shale, the deposition of lacustrine organic-rich shale was frequently influenced by multiple factors, including the changes in climate, lake level, and sediment supply (Jiang et al., 2016; Xu et al., 2017a). Lacustrine organic-rich shale thus generally shows a stronger heterogeneity and contains sandstone, siltstone, or limestone interlayers (Jiang et al., 2013; Ju et al., 2014; Wei et al., 2014). The strong heterogeneity not only affects the enrichment and evolution of organic matter but also challenges the fracturing stimulation and the sustainable high production (a high initial production but decreases rapidly). Considering the sandstone or limestone interlayers, the lacustrine organic-rich shale in the Ziliujing Formation can be subdivided into four members, including the Zhenzhuchong, Dongyuemiao, Maanshan, and Daanzhai members from the bottom to the top, respectively (Figure 1). Thereinto, the Daanzhai member has been hydraulically fractured to yield an initial gas rate of 1,500 m³ to 50 × 10⁴ m³ per day (Zou et al., 2019b), whereas the other members are still virgin land for shale gas production.

In this study, an investigation of the Dongyuemiao member was firstly conducted utilizing the macroscopic and microscopic analyses on outcrops and drilling cores in the eastern Sichuan Basin to reveal the spatial distribution of sedimentary subfacies and the characteristics of mineral compositions, organic matter content and types, thermal maturity level, and reservoir quality and then to evaluate the exploration prospect. Thorough knowledge of the lacustrine organic-rich shales in the Ziliujing Formation will aid in understanding the unique features of lacustrine shale, its reservoir quality, shale gas, or oil potential.

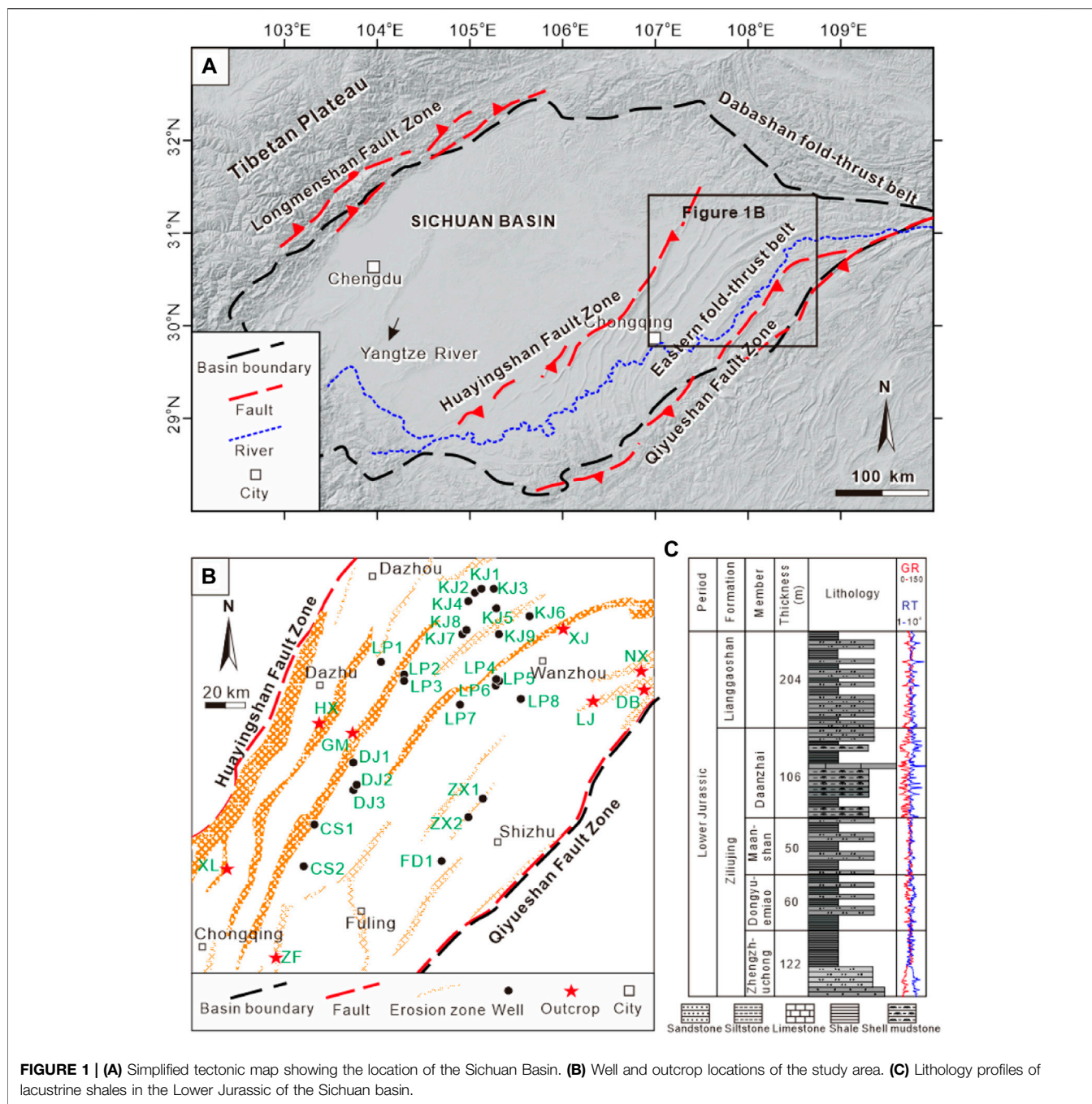
GEOLOGICAL SETTING

The Sichuan Basin, with a rhomboid shape, is located in southwest China (Figure 1). The basin behaved as an active margin from the middle Paleozoic to the Early Triassic (Dong et al., 2015). Intensive lateral compression has controlled tectonic activity in the basin since the middle Triassic, leading to the generation of fold-thrust belts on the northern and eastern boundary (Yan et al., 2000; Hao et al., 2008; Xu H. et al., 2019; Liu et al., 2019; Liu et al., 2020a; Liu et al., 2020b; Liu et al., 2021). Due to the re-compression derived from the Pacific Ocean plate in the Late Cenozoic, the eastern Sichuan Basin was intensely folded and regionally exhumed. Generally, the Sichuan Basin was dominated by marine deposition before the late Triassic and gradually transferred to the deposition of fluvial-lacustrine facies at the end of the Triassic (Reinhardt, 1988). The deposition center of early Jurassic lake was located in the eastern and northeastern Sichuan Basin.

The Early Jurassic Ziliujing formation of the eastern Sichuan Basin has a thickness of 100–400 m and consists of four members: the Zhenzhuchong, Dongyuemiao, Maanshan, and Daanzhai members from the bottom to the top (Li and He, 2014; Liu et al., 2020), respectively (Figure 1C). Because of the shallow water depth during the early lake flood, the Zhenzhuchong member is dominant by the interbeds of sandstone with mudstone and contains minor black shale (Guo et al., 2011; Guo et al., 2016). The continued lake transgression greatly elevated the water depth and enlarged the lake area, which benefited the deposition of black shale interbedding with thin intervals of sandstone or shell limestone in the Dongyuemiao member (Li et al., 2013; Tan et al., 2016). The Daanzhai member was deposited during the maximum flooding period and was dominated by black shale (Figure 2).

SAMPLES AND METHODS

A total of 54 rock samples of various sedimentary subfacies were obtained from outcrops and drilling cores, most of which were dark shale samples. Individual samples contain shell debris. Each sample will be divided into multiple parts for different experiments. A set of subsamples were crushed to fine powders (<100 μm) and analyzed for bulk rock properties, including bulk porosity (35 samples), mineralogical composition (15 samples), total organic carbon (TOC) content (41 samples), rock pyrolysis (41 samples), and carbon isotope analysis (11 samples). The bulk porosity of the samples was determined by measuring the grain volume under ambient conditions and the bulk volume by Archimedes' principle and by coupling of mercury immersion with a helium pycnometer (Pearson, 1999; Bustin et al., 2008; Chalmers et al., 2012). The difference between the bulk and grain volume was calculated as the bulk porosity. Random-powder x-ray diffraction (XRD) was used for mineralogical composition analysis using a Bruker D8 advance x-ray diffractometer at 40 kV and 30 mA with Cu Kα radiation. Stepped scanning measurements were performed at a rate of 4°/min with a range of 3°–85°. After the samples were



treated with 4% HCl to remove carbonates, the TOC content was measured using a Vario MACRO CHNS analyzer. The rock pyrolysis analyses were completed using a Rock-Eval VI Standard analyzer, and the amounts of free hydrocarbons (S_1) and pyrolysis hydrocarbons (S_2) and the temperature of the maximum pyrolysis yield (T_{max}) were obtained. The detailed operations of TOC content and rock pyrolysis analyses were following Espitalié et al. (1984). Rock samples for carbon isotope analysis were also decalcified with HCl, extracted with methylene chloride to remove bitumen, and dried at 90°C. Combustion to CO_2 was performed in an oxygen-helium atmosphere at 900°C

with copper oxide as catalyst. The evolved gas was purified over copper and silver at 600°C and transferred to a MAT-253 triple collector mass spectrometer. The results are reported as PDB standard.

Vitrinite reflectance (R_o) measurements were conducted on polished blocks under reflected light using a Leica MPV-SP microphotometric system following the procedures of Schoenherr et al. (2007). Small shale cubes were polished with argon ion milling at an acceleration voltage of 3 kV and a milling time of 2 h. Images were obtained by field emission scanning electron microscopy (FE-SEM) (Milliken et al., 2013).

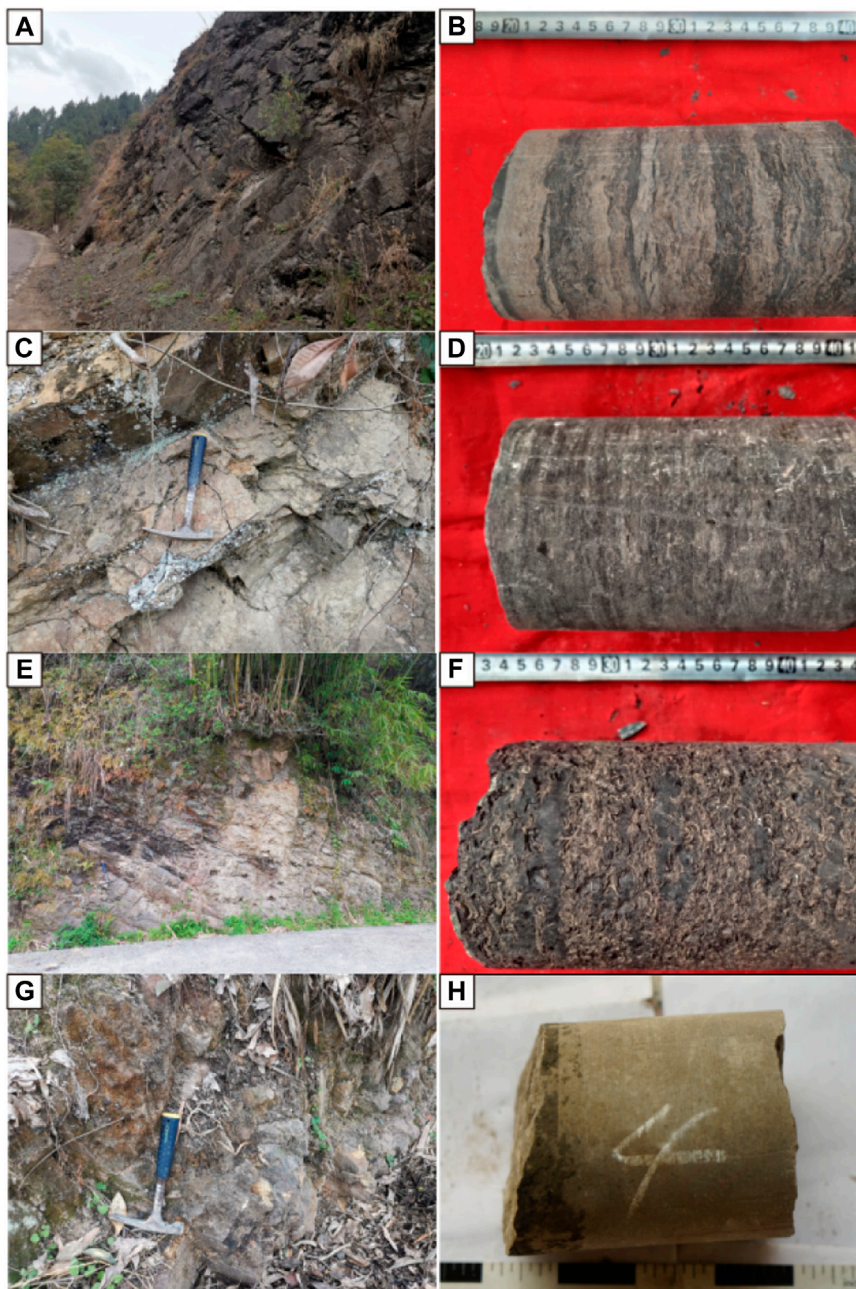


FIGURE 2 | Selected outcrop and drilling core photographs to show the characteristics of the lithology in four members. **(A)** Dark-gray sandstone interbedded with shell mudstone, the Daanzhai member in the outcrop NX. **(B)** Dark-gray shell limestone, the Daanzhai member of the well KJ5 (drilling cores). **(C)** Medium- to thick-bedded, sandstone interbedded with dark-gray shale, the Maanshan member in the outcrop DB. **(D)** Dark-gray silty mudstone with shell debris, the Maanshan member of the well CS1 (drilling cores). **(E)** Thin-bedded, dark-gray shale intercalated with light-gray to gray sandstone, the Dongyuemiao member in the outcrop HX. **(F)** Black shale interbedded with shell debris, the Dongyuemiao member of the well KJ6 (drilling cores). **(G)** Medium- to thick-bedded, light-gray siltstone, the Zhenzhuchong member in the outcrop XL. **(H)** The light-gray siltstone of the Zhenzhuchong member of the well FD1 (drilling cores). Please see **Figure 1B** for outcrop and well locations.

RESULTS

Sedimentary Subfacies and Characteristics

Deposits of the Dongyuemiao member can be grouped into four general subfacies categories based on texture, structure, and petrography: shore, shallow, semi-deep, and deep lacustrine

deposits (**Figure 3**). Shore lacustrine deposits primarily consist of light-gray to gray fine sandstone or siltstone with some horizontal or wavy laminations (**Figure 3B**), suggesting the high-energy condition with a relatively high oxygen concentration (Walker, 1967; Miall, 2013). The shallow lacustrine deposit consists of gray to dark-gray siltstone that is

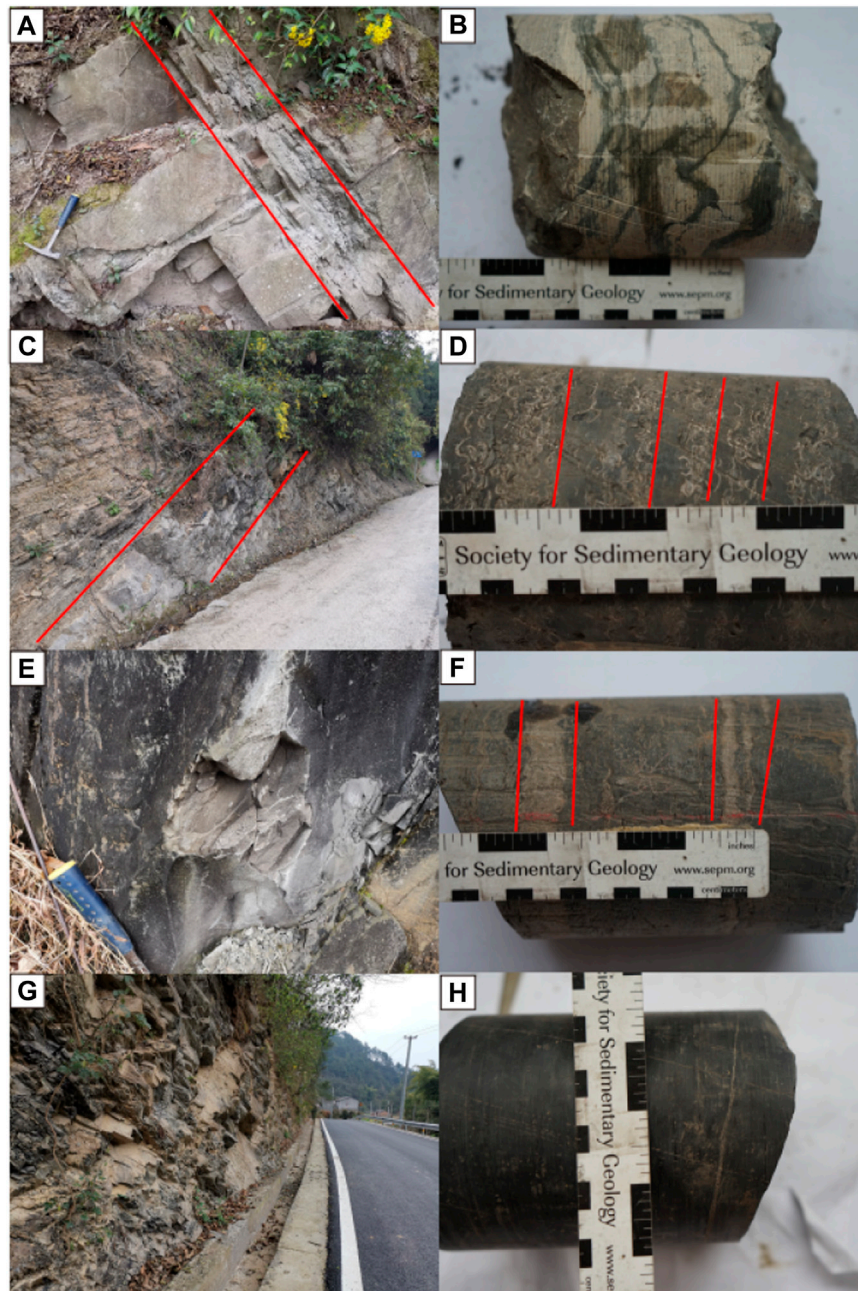


FIGURE 3 | Selected outcrop and drilling core photographs to show the characteristics of sedimentary subfacies in the Dongyuemiao member. **(A)** Medium- to thick-bedded, dark-gray sandstone from shore lake, the bottom of the outcrop LJ. **(B)** Light gray-green sandstone from shore lake, the well KJ5 (drilling cores). **(C)** Medium- to thick-bedded, gray sandstone from shallow lake, the bottom of the outcrop GM. **(D)** Gray mudstone contains shell debris from shallow lake, the well LP1 (drilling cores). **(E)** Gray siltstone from the semi-deep lake, the bottom of the outcrop XJ. **(F)** Gray mudstone interlayered shell debris from semi-deep lake, the well KJ3 (drilling cores). **(G)** Medium- to thick-bedded, gray siltstone and fine sandstone with some thin layers of gray-black shale from deep lake, the bottom of the outcrop ZF. **(H)** Black-gray shale from deep lake, the well LP8 (drilling cores). Please see **Figure 1B** for outcrop and well locations.

frequently interbedded with gray to dark-gray mudstone. Low-angle-inclined to horizontal laminations and bioclastic debris commonly appear in the siltstone and mudstone intervals, respectively (**Figure 3D**), suggesting a euphotic, oxidic, and circulating water setting. Shell debris in shale generally is the result of short-distance transportation by strong water energy,

which also can be verified by the biological disturbance structures. Semi-deep lacustrine deposit is characterized by thick-bedded, dark-gray to gray shale, which is frequently intercalated with banded or laminated shells. The increase of shale thickness relative to the shallow deposits suggests a low-energy and reducible water setting. Deep lacustrine deposit is dominated

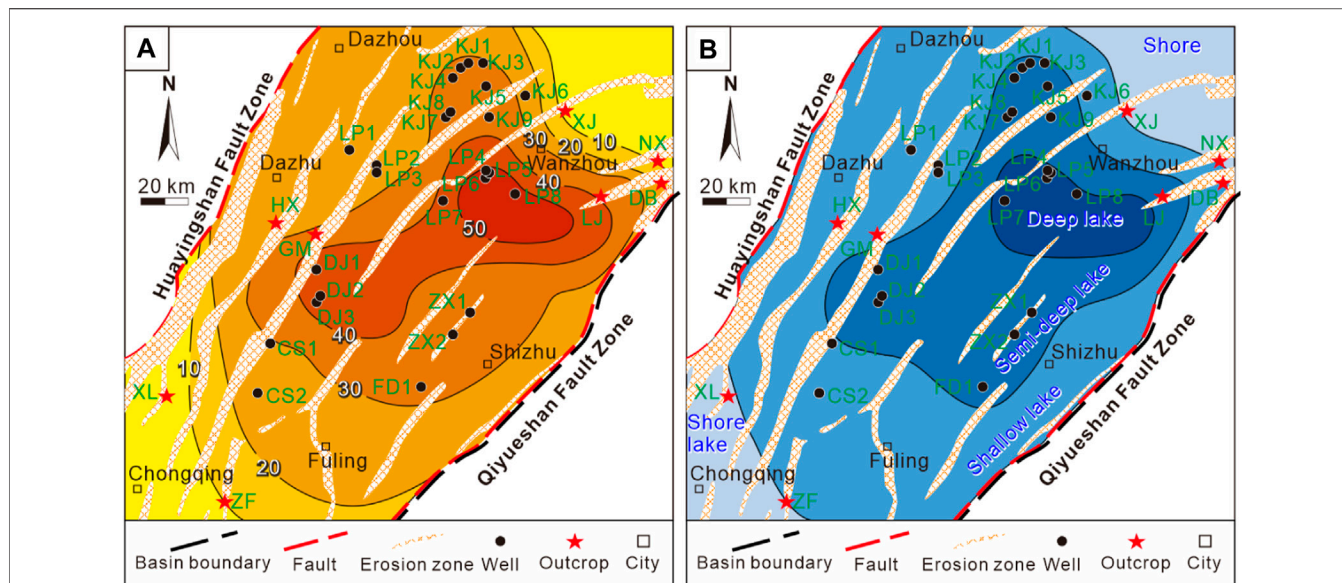


FIGURE 4 | (A) Dark shale thickness (in meters) and **(B)** sedimentary facies of the Dongyuemiao member. The thickness of dark shale is the largest in the southwest of Wanzhou City, reaching 50 m, where it is also the center of the lake basin during the deposition of the Dongyuemiao member.

TABLE 1 | Mineral compositions of black shale in the Dongyuemiao member in the eastern Sichuan Basin.

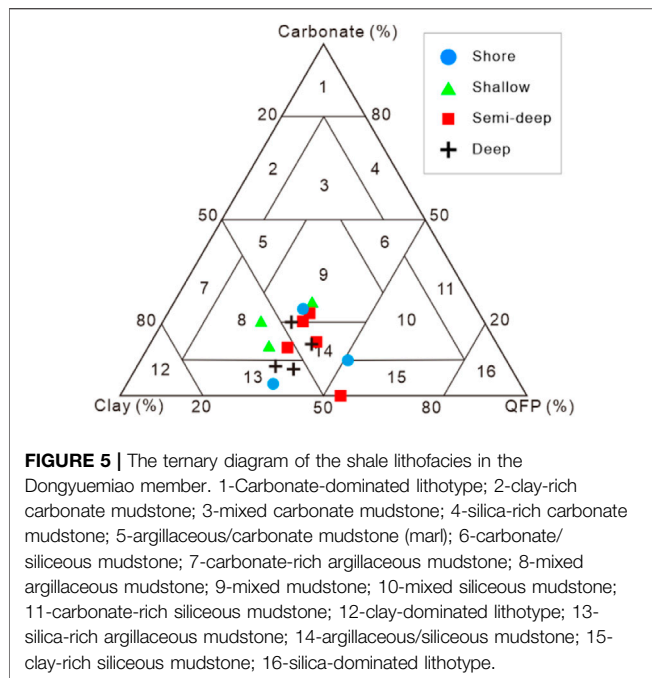
Well/outcrop	Minerals (wt.%)										Sedimentary surface
	Quartz	Feldspar	Calcite	Dolomite	Aragonite	Siderite	Halite	Pyrite	Hematite	Clay	
NX	31.1	4.5	2.4	\	\	0.7	0.5	\	\	60.8	Shore lake
XL	46.7	4.6	9.5	\	\	\	\	\	\	39.2	
XJ	28.2	3.5	23.6	\	\	2.5	\	\	\	42.2	
LP2	22.5	2.9	14.7	\	10	2.5	\	\	4.7	42.7	Shallow lake
CS2	29.7	1.2	19.4	\	7.4	1.2	\	\	1.6	39.5	
LP3	21.2	2.1	9.4	\	10.1	\	1.1	\	1.2	54.9	
ZX1	43.6	5.1	\	\	\	5.5	\	\	\	45.8	Semi-deep lake
KJ4	35.5	2.1	13.8	1.5	\	1.6	\	\	1.4	44.1	
DJ1	30.7	2.3	6.5	\	7.2	\	\	\	1.2	52.1	
KJ2	29.2	3	14.8	\	6.3	\	\	\	2.2	44.5	
FD1	25.9	2.1	14.2	\	\	\	\	\	1.5	56.3	
LP4	33.6	3	18	0.8	\	\	\	2.1	\	42.5	Deep lake
LP8	33.9	4.1	7.8	\	\	6.8	\	\	1.9	45.5	
LP6	27.6	4.7	8.8	\	\	\	\	1.5	\	57.4	
LP7	32.1	3.6	\	8	\	1.7	\	1.3	\	53.3	

by thick-bedded dark shale (Figure 3H). Generally, the shale thickness increases from the shore to deep lacustrine deposits. The sedimentary structure of deep lacustrine shale is mainly horizontal bedding. Integrating the total thickness of black shale (Figure 4A) and sedimentary textures and structures obtained from cores and outcrops, the regional distributions of the subfacies are as shown in Figure 4B, which indicates a deposition center located in the north-central part of the study area.

Mineral Compositions

The XRD analysis indicates that the black shale of the Dongyuemiao member is primarily composed of clay ranging

from 39.2 to 60.8 wt.% (at an average of 48.1 wt.%), quartz ranging from 21.2 to 46.7 wt.% (at an average of 31.4 wt.%), carbonates up to 26.8 wt.% (at an average of 14.8 wt.%), feldspar less than 5.1 wt.%, and minor heavy minerals (Table 1). Clay and quartz in the semi-deep and deep lacustrine shales generally exceed 40 and 30 wt.%, respectively. Carbonates, dominant by calcite, are relatively higher (>20 wt.%) in the shore and shallow lacustrine shales. The brittleness index estimated from mineral compositions presents an average value of 48.9%, but it varies with sedimentary subfacies. The average brittleness indexes of the shore, shallow, semi-deep, and deep lacustrine shales decrease by 51.4, 50.2, 48.7, and 46.5%, respectively. The content of brittle minerals is very important for fracturing stimulation



(Bustin et al., 2008; Tian et al., 2017; Xu et al., 2020). The brittleness index that can be estimated by the total brittle minerals (e.g., quartz, carbonate) content is generally more than 40%. Particularly, the appearance of shell debris increases the carbonate content of shale and increases the brittleness index of shale. The shale lithofacies identified from the ternary diagram (Gamero et al., 2013) indicate that the Dongyuemiao member belongs to the mixed argillaceous mudstone, mixed mudstone, silica-rich argillaceous mudstone, and argillaceous/ siliceous mudstone (Figure 5).

Porosity and Pore Structure

Helium porosity of black shale in the Dongyuemiao member generally ranges from 1.42 to 3.83% and presents an average value of 2.41% (Table 2). Shale porosity varies with sedimentary subfacies, showing average values of 2.14, 2.67, and 2.48% in the shallow, semi-deep, and deep lacustrine shales, respectively.

Pore networks in the black shale of the Dongyuemiao member are composed of fracture pores, mineral-matrix pores, and organic-matter pores (Figure 6). Multi-scales of fractures were not controlled by individual particles but were paralleling to the bedding surface and cemented by white calcite (Figure 6A). Mineral-matrix pores include interparticle and intraparticle mineral pores. Interparticle pores, with a variety of shapes ranging from elongated to rounded to angular, were generally scattered; for instance, the linear pore space between large clay platelets (Figure 6C) and the triangular pore space between rigid grains (e.g., pyrite) (Figure 6D). Intraparticle mineral pores were dominant by the carbonate dissolution pores, particularly the dissolution-rim moldic pores after partial or complete dissolved fossils (Figure 6E). Organic-matter pores, occurring as irregular, bubble-like, and elliptical pore space within organic matter and commonly ranging 1–50 nm in length, were widely identified (Figure 6F).

Organic Geochemical Characteristics

The total organic carbon (TOC) content in the black shale of the Dongyuemiao member generally ranges from 0.83 to 2.47 wt.% (Table 2). The average TOC content varies with sedimentary subfacies, showing average values of 1.36, 1.79, and 1.62% in the shallow, semi-deep, and deep lacustrine shales, respectively (Figure 7).

The rock pyrolysis results of the black shale of the Dongyuemiao member are present in Table 2. The free hydrocarbon content indicated by the S_1 value ranges 0.02–1.07 mg HC/g rock; the hydrocarbon-generating potential indicated by the S_2 value ranges from 0.18 to 12.90 mg HC/g rock. The majority of samples are thermally matured or highly matured as indicated by T_{max} ranging from 440°C to 507°C. The ratio of the hydrocarbon index [HI, $(100 \times S_2)/TOC$] to T_{max} indicates that most of the shale samples obtained from the Dongyuemiao member primarily contains type II kerogen with minor type III kerogen (Figure 8).

The carbon isotope of organic matter varies from –26.77‰ PDB to –24.62‰ PDB (Table 2), consisting of the typical ranges of type II (–25.5‰ PDB ~ –27.2‰ PDB) and III (–20.0‰ PDB to –26.0‰ PDB) kerogen (Huang et al., 1984).

The vitrinite reflectance (R_o) of the Dongyuemiao member varies from 0.89 to 1.77% (a thermal maturity from the gas-condensate window to gas window) (Table 2) and is linearly correlated with T_{max} (Figure 9). R_o generally increases from the west to the east of the study area (Figure 10).

DISCUSSION

Controlling Factors on Shale Porosity

Massive micro- to nanopores, particularly various shapes of pores in organic matters (i.e., organic-matter pore), were revealed in the organic-rich shale utilizing the high-resolution SEM in conjunction with other techniques, which made the organic-rich shale serve as both source and reservoir rock in the petroleum system (Loucks et al., 2012; Milliken et al., 2013; Yang et al., 2019). The positive correlation between TOC content and bulk porosity once suggested that the organic matter (OM) pores can be a dominant component of the pore system in the organic-rich shale (Xu et al., 2017b; Gao et al., 2018; Liu et al., 2020a). Nevertheless, there is no visible correlation between TOC content and porosity in the black shale of the Dongyuemiao member (Figure 11A).

OM pores were derived from the inheritance of primary bioorganic structure (i.e., primary OM pore) or secondarily generated by thermal cracking of organic matter (i.e., secondary OM pore). Primary OM pore rarely appears in the amorphous and ductile marine detrital OM (type II) as a consequence of burial compaction. Despite that the black shale of the Dongyuemiao member was deposited in the lacustrine environment, its organic matter was primarily categorized as type II that was unfavorable for inheriting primary OM pores (Figure 8). Because the primary pores (organic or inorganic) can be infilled by secondary OM (e.g., bitumen, solid bitumen, or migrabitumen) at a low thermal maturity level ($R_o < \sim 1.0\%$).

TABLE 2 | The results of total organic carbon (TOC), rock pyrolysis, vitrinite reflectance (R_o), carbon isotope of organic matter ($\delta^{13}C_{org}$), and porosity analyses on the black shale of the Dongyuemiao member in eastern Sichuan Basin.

Sample ID	Well/ outcrop	TOC (wt.%)	S_1	S_2	S_1 + S_2	HI (mg HC/g TOC)	T_{max} (°C)	R_o (%)	$\delta^{13}C_{org}$ (PDB ‰)	Porosity (%)	Sedimentary subface	
												(mg HC/g rock)
XJ-2	XJ	0.83	0.06	0.47	0.53	56.63	457	/	/	1.54	Shore lake	
ZF-1	ZF	1.05	0.02	0.44	0.46	41.74	448	/	/	1.62		
HX-1	HX	1.38	0.40	5.47	5.87	396.38	443	/	/	2.82	Shallow lake	
GM-2	GM	2.02	0.30	12.90	13.20	638.77	440	/	/	1.8		
DB-1	DB	1.08	0.05	0.73	0.77	67.15	480	/	/	1.68		
DB-2		1.13	0.27	1.91	2.18	169.34	455	/	/	1.62		
LJ-2	LJ	1.51	0.39	2.48	2.87	164.27	454	/	/	2.55		
CS2-2	CS2	1.17	0.95	2.00	2.95	170.68	452	1.48	/	1.95		
CS1-2	CS1	1.55	0.38	1.99	2.38	128.66	447	1.2	/	1.53		
LP1-2	LP1	1.51	0.43	1.14	1.57	75.70	444	1.04	/	1.73		
KJ6-2	KJ6	1.03	0.18	0.81	0.99	78.57	448	1.38	/	2.67		
LP2-2	LP2	1.52	0.50	3.53	4.02	232.03	442	0.89	/	1.88		
LP3-2	LP3	1.08	0.77	3.97	4.74	368.03	444	1.17	-26.32	3.32		
DJ1-2	DJ1	2.47	0.58	3.99	4.57	161.50	441	1.24	-26.76	1.99		Semi-deep lake
KJ9-2	KJ9	1.24	0.37	1.33	1.71	107.54	452	1.29	-26.51	2.11		
KJ9-1		1.58	0.17	0.80	0.97	50.51	440	/	/	/		
KJ1-2	KJ1	2.21	0.16	1.55	1.71	69.96	465	1.46	/	3.83		
KJ4-1	KJ4	1.05	0.20	0.88	1.08	84.12	458	1.23	-26.77	/		
KJ4-2		1.31	0.29	1.15	1.44	87.79	451	1.16	-26.5	1.65		
KJ5-1	KJ5	1.55	0.10	0.74	0.84	47.74	473	1.48	-25.63	3.55		
KJ3-1	KJ3	1.43	0.08	1.41	1.48	98.39	500	1.36	/	2.32		
DJ3-1	DJ3	2.33	0.20	3.76	3.96	161.37	442	1.32	/	2.17		
DJ3-3		1.98	0.60	4.56	5.17	230.49	439	1.21	/	2.96		
ZX1-2	ZX1	1.82	0.13	0.39	0.52	21.52	497	1.77	/	3.13		
ZX2-3	ZX2	1.48	0.05	1.13	1.19	76.64	489	1.58	-24.62	2.52		
KJ8-2	KJ8	1.93	0.10	4.52	4.62	234.12	445	1.18	/	2.82		
KJ2-2	KJ2	1.89	0.19	3.57	3.76	188.96	460	1.43	-25.71	2.96		
KJ7-2	KJ7	1.87	0.08	2.64	2.72	141.04	450	1.41	/	3.17		
FD1-2	FD1	1.84	0.38	0.18	0.57	9.88	507	1.77	-25.7	2.25		
DJ2-2	DJ2	2.46	0.54	4.30	4.84	174.69	448	1.3	/	2.68		
LP7-2	LP7	1.72	0.60	2.40	3.00	139.43	384	1.34	/	3.45	Deep lake	
LP6-3	LP6	1.88	0.84	2.51	3.35	133.25	470	1.47	/	/		
LP6-2		1.42	0.15	0.81	0.97	57.24	750	1.46	/	1.53		
LP6-1		1.54	0.79	2.02	2.81	131.19	462	1.56	/	/		
LP4-2	LP4	1.52	0.19	0.67	0.87	44.39	450	1.38	/	1.42		
LP5-1	LP5	1.43	0.46	0.80	1.27	56.17	445	1.54	/	1.66		
LP5-2		1.55	0.19	1.55	1.74	100.08	444	/	/	/		
LP8-2	LP8	1.95	1.07	2.75	3.82	140.77	449	1.34	/	/		
LP8-3		1.59	0.67	1.49	2.15	93.43	462	1.07	-26.26	3.01		
LP8-8		1.77	0.95	1.73	2.68	97.58	464	1.35	-25.34	2.69		
LP8-13		1.49	0.63	1.43	2.05	95.95	469	1.27	/	3.63		

Secondary OM pores were primarily generated during the gas window; in other words, the thermal maturity level indicated by R_o should exceed $\sim 1.0\%$. Dramatically, the thermal maturity levels of black shale in the Dongyuemiao member generally exceed $\sim 1.0\%$ (Figures 8–10). A cross plot of porosity with T_{max} was adapted to reveal the influence of thermal cracking on shale porosity (Figure 11B). The majority of black shale samples in the Dongyuemiao member show a positive correlation between porosity and T_{max} when the T_{max} ranges from $\sim 440^\circ\text{C}$ to $\sim 465^\circ\text{C}$. This correlation consists of the tendency of Posidonia Shale (Type II) (Han et al., 2017) and seems to suggest the thermally driven pore generation, e.g., the secondary

OM pore. However, as T_{max} exceeds $\sim 465^\circ\text{C}$, there is a negative correlation between porosity and T_{max} (Figure 11B), implying some pore destruction mechanisms at high thermal maturity levels.

According to the conclusion of Han et al. (2017), the generation of secondary OM pore was accompanied by the decrease of oil retention capacity. Notably, except for highly matured samples ($T_{max} > \sim 465^\circ\text{C}$), the oil saturation index [OSI=(100 × S_1)/TOC] positively correlates with porosity in the black shale of the Dongyuemiao member (Figure 11C), implying good hydrocarbon retention of thermally generated pores. The OSI values of highly matured samples

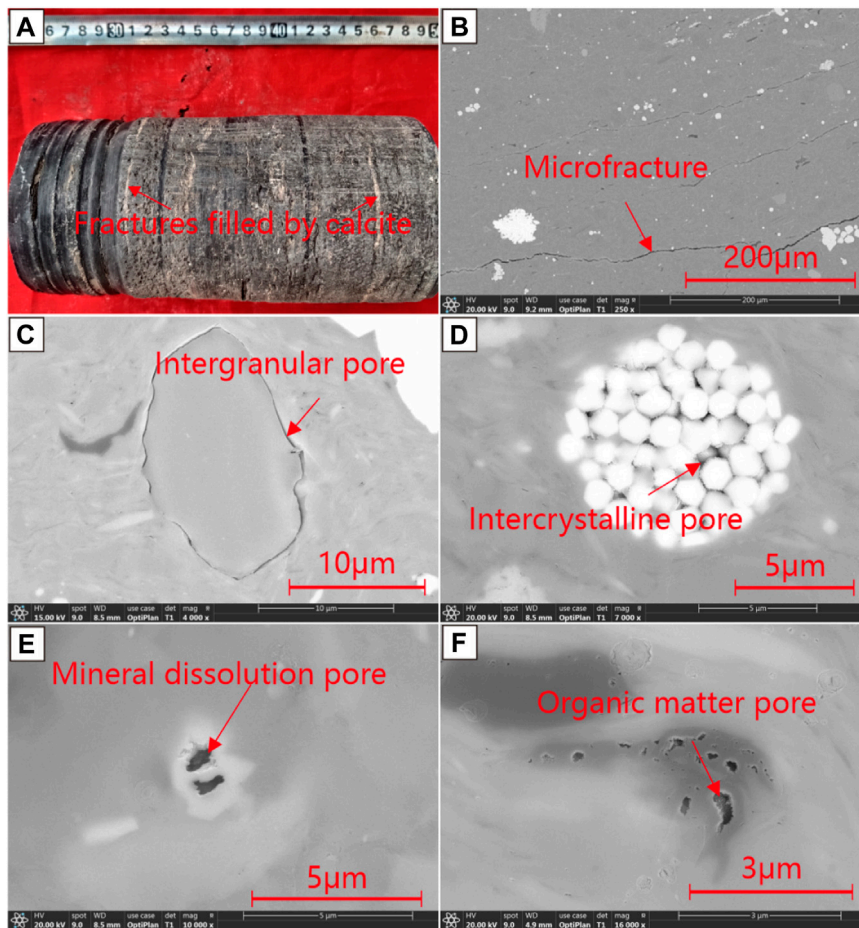


FIGURE 6 | (A) Fractures are filled with white calcite (B) microfracture, (C) intergranular pore between large clay platelets (D) triangular intercrystalline pore of pyrite, (E) mineral dissolution pore, and (F) irregular, bubble-like organic-matter pore in the black shale of the Dongyuemiao member.

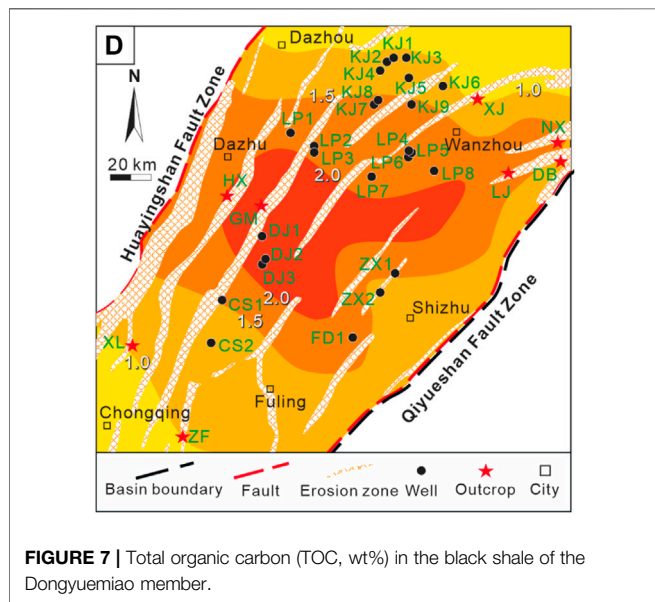
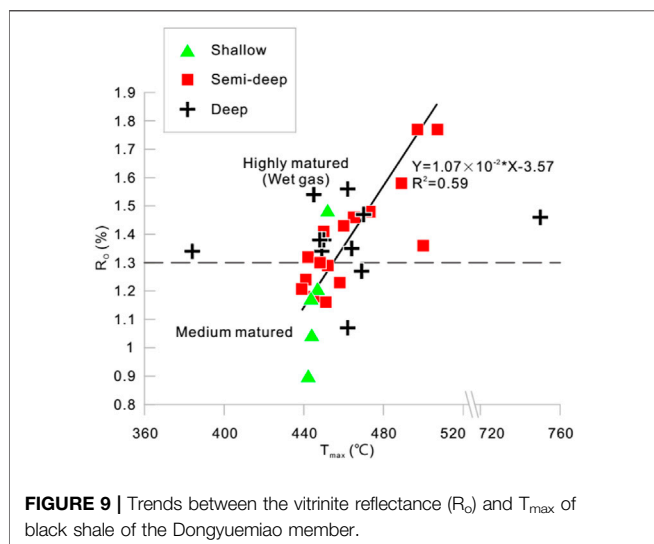
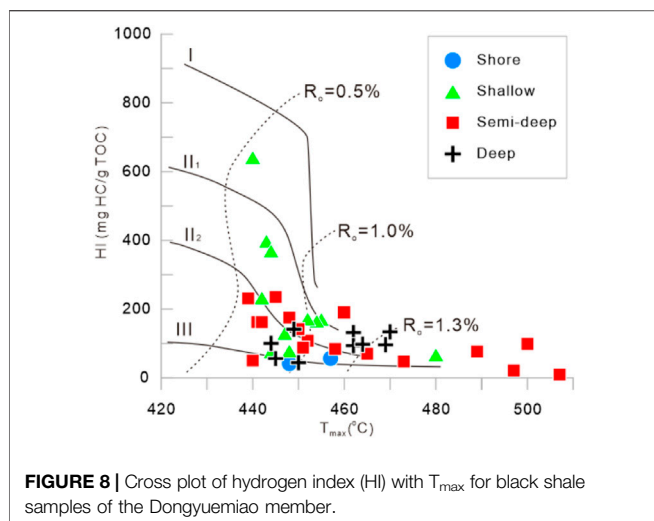


FIGURE 7 | Total organic carbon (TOC, wt%) in the black shale of the Dongyuemiao member.

($T_{max} > \sim 465^{\circ}\text{C}$) are less than 10 mg HC/g TOC (Figure 11C), indicating a strong hydrocarbon expulsion. Considering the multi-scales of healed and unhealed fractures identified in cores and outcrops (Figures 6A,B), we suspected that fractures may account for the abnormally high porosity in samples of $T_{max} > \sim 465^{\circ}\text{C}$ which also promoted the hydrocarbon expulsion and subsequently the healing of fractures by with calcite decrease the shale porosity.

Shale Gas Exploration Prospect

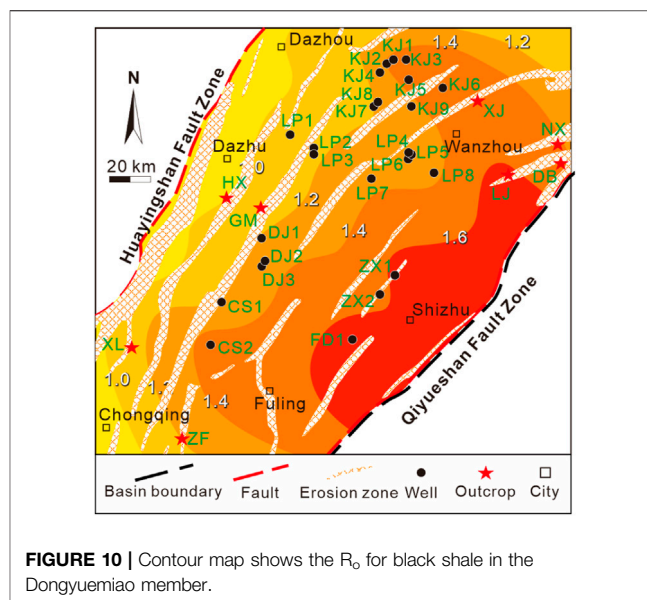
Due to the low-energy and anoxic setting that was indicated by the horizontal lamination or even lack of lamination, the black shales of semi-deep and deep lacustrine subfacies in the Dongyuemiao member generally have a TOC content greater than 1.5% (Table 2; Figure 12A), which can be classified as the good source rock following the standard of (Qin, 2005) but is slightly less than the average TOC content of 2.0% in the “sweet point” of the overlying Daanzhai member (Zou et al., 2019b). In contrast, the vast majority of shales samples obtained from shore and shallow lacustrine subfacies in the Dongyuemiao member have a TOC content less than 1.5%. The higher TOC content in



the semi-deep and deep lacustrine shales generally yielded higher values in the hydrocarbon generating potential ($S_1 + S_2$) (Figure 12A).

Nevertheless, the OSI values of some semi-deep lacustrine shale samples are abnormally low (<30 mg HC/g TOC) at high TOC content (>1.8 wt.%) (Figure 12B). These low OSI samples are coupling with high T_{max} magnitudes (>470°C) (Figure 12C), which indicates that these samples are primarily located in the eastern of the study area, i.e., in the vicinity of the Qiyueshan Fault Zone (Figure 10). The risk of hydrocarbon leakage from the semi-deep lacustrine shale in the vicinity of the Qiyueshan Fault Zone thus cannot be neglected (Xu S. et al., 2019).

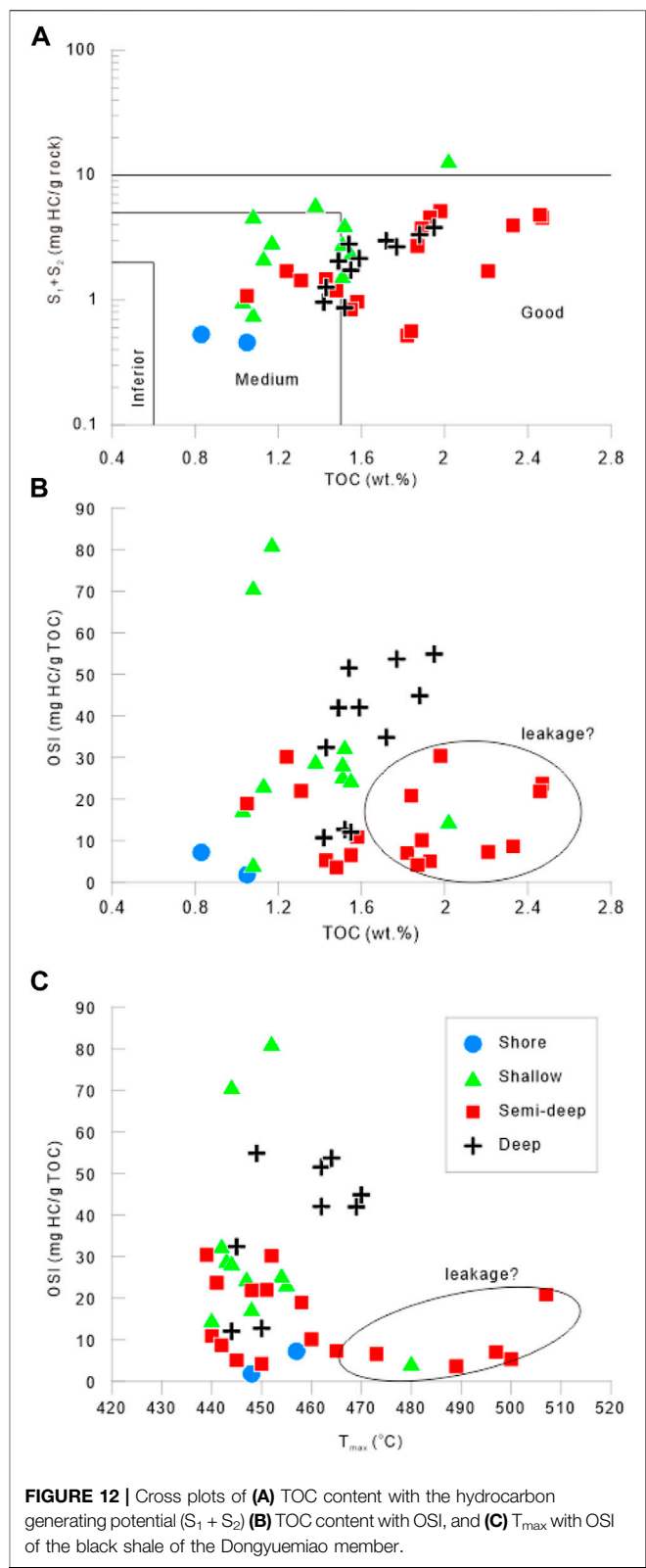
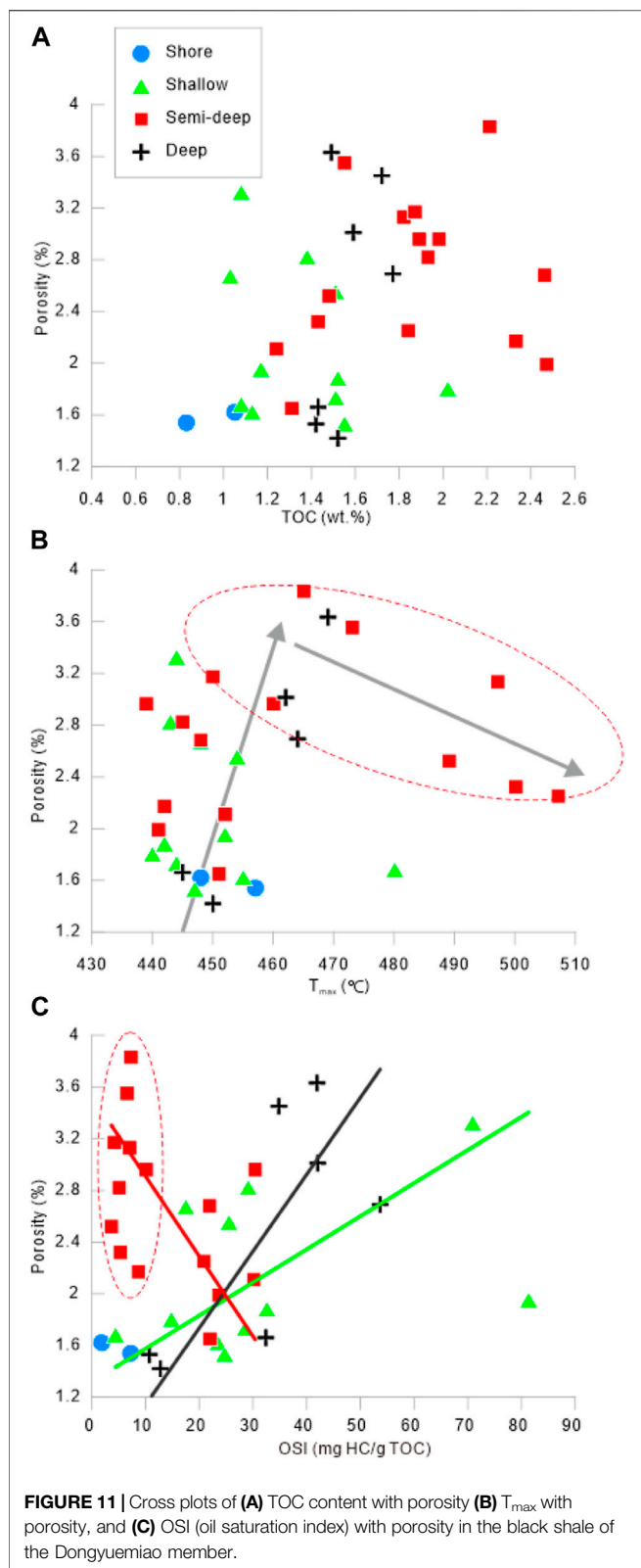
The clay mineral contents of the semi-deep and deep lacustrine shales are generally higher than 40 wt.% (Figure 5), which challenges the artificial hydraulic fracturing by 1) the decrease of brittleness index and inhibition of open and propagation of hydraulic fractures (Tian et al., 2017) and 2) the interactions between clay



minerals and hydraulic fracturing fluids, including water-blocking effect, shale swelling, and mineral dissolution and precipitation (Lyu et al., 2015; Herz-Thyhsen et al., 2020). The silty mudstone or siltstone interlayers in the semi-deep lacustrine shales can either promote or inhibit the fracture propagation that may depend on the *in-situ* stress state of various structural domains.

CONCLUSION

The dark shales in the Dongyuemiao member can be grouped into four general categories: shore, shallow, semi-deep, and deep lacustrine shales. The shore lacustrine shale generally has a very thin thickness, with an average TOC content of 0.94 wt%, average brittle mineral content of 51.4 wt%, and average porosity of 1.58%; shallow lacustrine shale has a thickness up to 20 m, average TOC content of 1.36 wt%, average brittle mineral content of 50.2 wt%, and average porosity of 2.19%; semi-deep lacustrine shale has a thickness up to 50 m, average TOC content of 1.79 wt%, average brittle mineral content of 48.7 wt%, and average porosity of 2.68%; and deep lacustrine shale has thickness more than 50 m, average TOC content of 1.62 wt%, average brittle mineral content of 46.5 wt%, and average porosity of 2.23%. All four categories of shales primarily consist of type II kerogen and have thermal maturity levels exceeding the vitrinite reflectance value of 0.9–1.0% (or the T_{max} of ~440°C). Thermally powered pore generation generally promoted the pore system as indicated by the positive correlation between porosity and T_{max} . Notably, the semi-deep lacustrine shale in the vicinity of the Qiyueshan Fault Zone shows abnormally high porosity and low OSI at $T_{max} > \sim 465^\circ\text{C}$ potentially due to the promoted hydrocarbon expulsion through multiscale fractures. Except for the



vicinity of the Qiyueshan Fault Zone, the semi-deep and deep lacustrine shales generally show the better exploration prospect relative to the shore and shallow lacustrine shales.

Additionally, the high content of clay minerals (>40 wt%) reduced the brittleness of the semi-deep and deep lacustrine shales which may challenge the artificial hydraulic fracturing.

DATA AVAILABILITY STATEMENT

The original contributions presented in the study are included in the article/Supplementary Material, further inquiries can be directed to the corresponding authors.

AUTHOR CONTRIBUTIONS

GW completed the writing and editing of the article. WW and XT designed the research and focused on the scientific issues involved in the article. LF provided the shale samples. CY, ZZ, HZ, and SW performed the data analyses and prepared the figures and tables. All authors contributed to the article and approved the submitted version.

REFERENCES

- Bustin, R., Bustin, A., Cui, A., Ross, D., and Pathi, V. (2008). "Impact of Shale Properties on Pore Structure and Storage Characteristics," SPE Paper. 119892 in Paper Presented at the Society of Petroleum Engineers shale Gas Production Conference in Fort Worth, Texas, Fort Worth, TX.
- Chalmers, G. R., Bustin, R. M., and Power, I. M. (2012). Characterization of Gas Shale Pore Systems by Porosimetry, Pycnometry, Surface Area, and Field Emission Scanning Electron Microscopy/transmission Electron Microscopy Image Analyses: Examples from the Barnett, Woodford, Haynesville, Marcellus, and Doig Units. *Bulletin* 96 (6), 1099–1119. doi:10.1306/10171111052
- Chen, Y., Xu, J., and Wang, P. (2020). Shale Gas Potential in China: A Production Forecast of the Wufeng-Longmaxi Formation and Implications for Future Development. *Energy Policy* 147, 111868. doi:10.1016/j.enpol.2020.111868
- Dong, D., Gao, S., Huang, J., Guan, Q., Wang, S., and Wang, Y. (2015). Discussion on the Exploration & Development prospect of Shale Gas in the Sichuan Basin. *Nat. Gas Industry B* 2 (1), 9–23. doi:10.1016/j.ngib.2015.02.002
- Dong, D., Shi, Z., Guan, Q., Jiang, S., Zhang, M., Zhang, C., et al. (2018). Progress, Challenges and Prospects of Shale Gas Exploration in the Wufeng-Longmaxi Reservoirs in the Sichuan Basin. *Nat. Gas Industry B* 5 (5), 415–424. doi:10.1016/j.ngib.2018.04.011
- Dong, T., Harris, N. B., Ayranci, K., and Yang, S. (2017). The Impact of Rock Composition on Geomechanical Properties of a Shale Formation: Middle and Upper Devonian Horn River Group Shale, Northeast British Columbia, Canada. *Bulletin* 101, 177–204. doi:10.1306/07251615199
- Espitalié, J., Marquis, F., and Barsony, I. (1984). "Geochemical Logging," in *Analytical Pyrolysis*. Editor K. J. Voorhess (Boston: Butterworths), 53–79.
- Gamero, H., Miller, C., and Lewis, R. (2013). "sCore: a Mineralogy Based Classification Scheme for Organic Mudstones," in SPE Annual Technical Conference and Exhibition, New Orleans, Louisiana, USA, September 2013.
- Gao, Z., Yang, S., Jiang, Z., Zhang, K., and Chen, L. (2018). Investigating the Spontaneous Imbibition Characteristics of continental Jurassic Ziliujing Formation Shale from the Northeastern Sichuan Basin and Correlations to Pore Structure and Composition. *Mar. Pet. Geology*. 98, 697–705. doi:10.1016/j.marpetgeo.2018.09.023
- Guo, T., Li, Y., and Wei, Z. (2011). Reservoir Forming Conditions of Shale Gas in Ziliujing Formation of Yuanba Area in Sichuan Basin. *Nat. Gas Geosci.* 22 (1), 1–7. (in Chinese).
- Guo, X., Hu, D., Li, Y., Wei, X., Liu, R., Liu, Z., et al. (2016). Analyses and Thoughts on Accumulation Mechanisms of marine and Lacustrine Shale Gas: A Case Study in Shales of Longmaxi Formation and Daanzhai Section of Ziliujing Formation in Sichuan Basin. *Earth Sci. Front.* 23 (2), 18, 2016. (in Chinese).
- Han, Y., Horsfield, B., Wirth, R., Mahlstedt, N., and Bernard, S. (2017). Oil Retention and Porosity Evolution in Organic-Rich Shales. *AAPG Bull.* 101 (6), 807–827. doi:10.1306/09221616069
- Hao, F., Guo, T., Zhu, Y., Cai, X., Zou, H., and Li, P. (2008). Evidence for Multiple Stages of Oil Cracking and Thermochemical Sulfate Reduction in the Puguang

FUNDING

This research was supported by the Fund of Key Laboratory of Shale Gas Exploration, Ministry of Natural Resources (Grant Number KLSGE-MLR-2020001), and the Science and Technology Cooperation Project of the CNPC-SWPU Innovation Alliance (Grant Number 2020CX0103020).

ACKNOWLEDGMENTS

We acknowledge the PetroChina Southwest Oil and Gas Field Company for sample collection.

- Gas Field, Sichuan Basin, China. *Bulletin* 92 (5), 611–637. doi:10.1306/01210807090
- He, F., and Zhu, T. (2012). Favorable Targets of Breakthrough and Built-Up of Shale Gas in continental Facies in Lower Jurassic, Sichuan Basin. *Petrol. Geol. Exp.* 34 (3), 246–251.
- Herz-Thyhsen, R. J., Kaszuba, J. P., and Dewey, J. C. (2020). Mineral Dissolution and Precipitation Induced by Hydraulic Fracturing of a Mudstone and a Tight sandstone in the Powder River Basin, Wyoming, USA. *Appl. Geochem.* 119, 104636. doi:10.1016/j.apgeochem.2020.104636
- Huang, D., Li, J., and Zhang, D. (1984). Kerogen Types and Study on Effectiveness, Limitation and Interrelation of Their Identification Parameters. *Acta Sedimentol. Sin.* 3, 18–33. (in Chinese).
- Jiang, S., Henriksen, S., Wang, H., Lu, Y., Ren, J., Cai, D., et al. (2013). Sequence-stratigraphic Architectures and Sand-Body Distribution in Cenozoic Rifted Lacustrine Basins, east China. *Bulletin* 97 (9), 1447–1475. doi:10.1306/03041312026
- Jiang, S., Xu, Z., Feng, Y., Zhang, J., Cai, D., Chen, L., et al. (2016). Geologic Characteristics of Hydrocarbon-Bearing marine, Transitional and Lacustrine Shales in China. *J. Asian Earth Sci.* 115, 404–418. doi:10.1016/j.jseaes.2015.10.016
- Ju, Y., Wang, G., Bu, H., Li, Q., and Yan, Z. (2014). China Organic-Rich Shale Geologic Features and Special Shale Gas Production Issues. *J. Rock Mech. Geotechnical Eng.* 6 (3), 196–207. doi:10.1016/j.jrmge.2014.03.002
- Li, Y., Feng, Y., Liu, H., Zhang, L., and Zhao, S. (2013). Geological Characteristics and Resource Potential of Lacustrine Shale Gas in the Sichuan Basin, SW China. *Pet. Exploration Development* 40 (4), 454–460. doi:10.1016/s1876-3804(13)60057-9
- Li, Y., and He, D. (2014). Evolution of Tectonic-Depositional Environment and Prototype Basins of the Early Jurassic in Sichuan Basin and Adjacent Areas. *Acta Pet. Sin.* 35 (2), 219–232. (in Chinese).
- Li, Y., Shao, D., Lv, H., Zhang, Y., Zhang, X., and Zhang, T. (2015). A Relationship between Elemental Geochemical Characteristics and Organic Matter Enrichment in marine Shale of Wufeng Formation-Longmaxi Formation, Sichuan Basin. *Acta Pet. Sin.* 36 (12), 1470–1483.
- Liu, J., Yao, Y., Liu, D., and Elsworth, D. (2017). Experimental Evaluation of CO₂ Enhanced Recovery of Adsorbed-Gas from Shale. *Int. J. Coal Geology*. 179, 211–218. doi:10.1016/j.coal.2017.06.006
- Liu, R., Hao, F., Engelder, T., Shu, Z., Yi, J., Xu, S., et al. (2019). Stress Memory Extracted from Shale in the Vicinity of a Fault Zone: Implications for Shale-Gas Retention. *Mar. Pet. Geology*. 102, 340–349. doi:10.1016/j.marpetgeo.2018.12.047
- Liu, R., Hao, F., Engelder, T., Zhu, Z., Yi, J., Xu, S., et al. (2020a). Influence of Tectonic Exhumation on Porosity of Wufeng-Longmaxi Shale in the Fuling Gas Field of the Eastern Sichuan Basin, China. *Bulletin* 104 (4), 939–959. doi:10.1306/08161918071
- Liu, R., Jiang, D., Zheng, J., Hao, F., Jing, C., Liu, H., et al. (2021). Stress Heterogeneity in the Changing Shale-Gas Field, Southern Sichuan Basin: Implications for a Hydraulic Fracturing Strategy. *Mar. Pet. Geology*. 132, 105218. doi:10.1016/j.marpetgeo.2021.105218

- Liu, R., Zheng, J., Hao, F., Nie, Z., Heng, D., Tan, X., et al. (2020b). Variation in Pore Systems with Tectonic Stress in the Overthrust Wufeng-Longmaxi Shale of the Southern Sichuan Basin, China. *J. Nat. Gas Sci. Eng.* 83, 103617. doi:10.1016/j.jngse.2020.103617
- Liu, Z., Liu, G., Hu, Z., Feng, D., Zhu, T., Bian, R., et al. (2020). Lithofacies Types and Assemblage Features of continental Shale Strata and Their Implications for Shale Gas Exploration: A Case Study of the Middle and Lower Jurassic Strata in the Sichuan Basin. *Nat. Gas Industry B* 7 (4), 358–369. doi:10.1016/j.ngib.2019.12.004
- Loucks, R. G., Reed, R. M., Ruppel, S. C., and Hammes, U. (2012). Spectrum of Pore Types and Networks in Mudrocks and a Descriptive Classification for Matrix-Related Mudrock Pores. *Bulletin* 96 (6), 1071–1098. doi:10.1306/08171111061
- Lyu, Q., Ranjith, P. G., Long, X., Kang, Y., and Huang, M. (2015). A Review of Shale Swelling by Water Adsorption. *J. Nat. Gas Sci. Eng.* 27, 1421–1431. doi:10.1016/j.jngse.2015.10.004
- Miall, A. D. (2013). *Principles of Sedimentary Basin Analysis*. Springer Science & Business Media, 146–148.
- Milliken, K. L., Rudnicki, M., Awwiller, D. N., and Zhang, T. (2013). Organic Matter-Hosted Pore System, Marcellus Formation (Devonian), Pennsylvania. *Bulletin* 97 (2), 177–200. doi:10.1306/07231212048
- Pearson, F. J. (1999). What Is the Porosity of a Mudrock? *Geol. Soc. Lond. Spec. Publications* 158 (1), 9–21. doi:10.1144/gsl.sp.1999.158.01.02
- Qin, J. (2015). *Petroleum Source Rock of China*. Beijing: China Science Publishing & Media, 116–168.
- Qiu, Z., Zou, C., Wang, H., Dong, D., Lu, B., Chen, Z., et al. (2020). Discussion on the Characteristics and Controlling Factors of Differential Enrichment of Shale Gas in the Wufeng-Longmaxi Formations in south China. *J. Nat. Gas Geosci.* 5 (3), 117–128. doi:10.1016/j.jnggs.2020.05.004
- Reinhardt, J. W. (1988). Uppermost Permian Reefs and Permo-Triassic Sedimentary Facies from the southeastern Margin of Sichuan Basin, China. *Facies* 18 (1), 231–287. doi:10.1007/bf02536802
- Schoenherr, J., Littke, R., Urai, J. L., Kukla, P. A., and Rawahi, Z. (2007). Polyphase thermal Evolution in the Infra-cambrian Ara Group (South Oman Salt Basin) as Deduced by Maturity of Solid Reservoir Bitumen. *Org. Geochem.* 38 (8), 1293–1318. doi:10.1016/j.orggeochem.2007.03.010
- Tan, M., Liu, Z., Shen, F., Xie, R., Liu, C., Deng, K., et al. (2016). Features and Model of Mixed Sediments of Da'anzhai Member in Lower Jurassic Ziliujing Formation, Huilong Area, Sichuan Basin. *Acta Sedimentol. Sin.* 34 (3), 571–581. (in Chinese).
- Walker, R. G. (1967). Turbidite Sedimentary Structures and Their Relationship to Proximal and Distal Depositional Environments. *J. Sediment. Res.* 37 (1), 25–43. doi:10.1306/74d71645-2b21-11d7-8648000102c1865d
- Wang, Y., Dong, D., Li, X., Huang, J., Wang, S., and Wu, W. (2015). Stratigraphic Sequence and Sedimentary Characteristics of Lower Silurian Longmaxi Formation in Sichuan Basin and its Peripheral Areas. *Nat. Gas Industry B* 2 (2-3), 222–232. doi:10.1016/j.ngib.2015.07.014
- Wei, X., Huang, J., Li, Y., Wang, Q., Liu, R., and Wen, Z. (2014). The Main Factors Controlling the Enrichment and High Production of Da'anzhai Member continental Shale Gas in Yuanba Area. *Geol. China.* 41 (3), 970–981. (in Chinese).
- Xu, H., Zhou, W., Zhang, R., Liu, S., and Zhou, Q. (2019a). Characterizations of Pore, mineral and Petrographic Properties of marine Shale Using Multiple Techniques and Their Implications on Gas Storage Capability for Sichuan Longmaxi Gas Shale Field in China. *Fuel* 241, 360–371. doi:10.1016/j.fuel.2018.12.035
- Xu, Q., Liu, B., Ma, Y., Song, X., Wang, Y., and Chen, Z. (2017b). Geological and Geochemical Characterization of Lacustrine Shale: a Case Study of the Jurassic Da'anzhai Member Shale in the central Sichuan Basin, Southwest China. *J. Nat. Gas Sci. Eng.* 47, 124–139. doi:10.1016/j.jngse.2017.09.008
- Xu, Q., Liu, B., Ma, Y., Song, X., Wang, Y., Xin, X., et al. (2017a). Controlling Factors and Dynamical Formation Models of Lacustrine Organic Matter Accumulation for the Jurassic Da'anzhai Member in the Central Sichuan Basin, Southwestern China. *Mar. Pet. Geology.* 86, 1391–1405. doi:10.1016/j.marpetgeo.2017.07.014
- Xu, S., Hao, F., Shu, Z., Zhang, A., and Yang, F. (2020). Pore Structures of Different Types of Shales and Shale Gas Exploration of the Ordovician Wufeng and Silurian Longmaxi Successions in the Eastern Sichuan Basin, South China. *J. Asian Earth Sci.* 193, 104271. doi:10.1016/j.jseae.2020.104271
- Xu, S., Liu, R., Hao, F., Engelder, T., Yi, J., Zhang, B., et al. (2019b). Complex Rotation of Maximum Horizontal Stress in the Wufeng-Longmaxi Shale on the Eastern Margin of the Sichuan Basin, China: Implications for Predicting Natural Fractures. *Mar. Pet. Geology.* 109, 519–529. doi:10.1016/j.marpetgeo.2019.06.008
- Yan, D., Wang, X., and Liu, Y. (2000). Analysis of Fold Style and Its Formation Mechanism in the Area of Boundary Among Sichuan, Hubei and Hunan. *Geoscience* 2000 (01), 37–43. (in Chinese).
- Yang, R., Hu, Q., Yi, J., Zhang, B., He, S., Guo, X., et al. (2019). The Effects of mineral Composition, TOC Content and Pore Structure on Spontaneous Imbibition in Lower Jurassic Dongyuemiao Shale Reservoirs. *Mar. Pet. Geology.* 109, 268–278. doi:10.1016/j.marpetgeo.2019.06.003
- Zhang, J., Nie, H., Xu, B., Jiang, S., Zhang, P., and Wang, Z. Y. (2008). Geological Condition of Shale Gas Accumulation in Sichuan Basin. *Nat. Gas Indust.* 28 (2), 151–156.
- Zou, C., Yang, Z., Wang, H., Dong, D., Liu, H., Shi, Z., et al. (2019a). Exploring Petroleum inside Source Kitchen': Jurassic Unconventional continental Giant Shale Oil & Gas Field in Sichuan basin, China. *Acta Geol. Sin.* 93 (07), 1551–1562. (in Chinese).
- Zou, C., Zhu, R., Chen, Z.-Q., Ogg, J. G., Wu, S., Dong, D., et al. (2019b). Organic-matter-rich Shales of China. *Earth-Science Rev.* 189, 51–78. doi:10.1016/j.earscirev.2018.12.002

Conflict of Interest: Author LF was employed by the company PetroChina Southwest Oil and Gas Field.

The remaining authors declare that the research was conducted in the absence of any commercial or financial relationships that could be construed as a potential conflict of interest.

Publisher's Note: All claims expressed in this article are solely those of the authors and do not necessarily represent those of their affiliated organizations, or those of the publisher, the editors, and the reviewers. Any product that may be evaluated in this article, or claim that may be made by its manufacturer, is not guaranteed or endorsed by the publisher.

Copyright © 2021 Wei, Wang, Feng, Tan, Yu, Zhang, Zhang and Wang. This is an open-access article distributed under the terms of the Creative Commons Attribution License (CC BY). The use, distribution or reproduction in other forums is permitted, provided the original author(s) and the copyright owner(s) are credited and that the original publication in this journal is cited, in accordance with accepted academic practice. No use, distribution or reproduction is permitted which does not comply with these terms.